Unlocking the Microstructure of Inhalation Blends using X-ray Microscopy

Parmesh Gajjar,[1] Hrishikesh Bale,[2] Timothy L. Burnett,[1] Xizhong Chen,[3] James A. Elliott,[3] Herminso Villarraga-Gomez,[4] Robert Hammond,[5] Hien Nguyen,[5] Kevin Roberts,[5] Ioanna Danai Styliari,[6] Benjamin Tordoff,[7] Philip J Withers[1] and Darragh Murnane[6]

[1] Henry Moseley X-ray Imaging Facility, School of Materials, University of Manchester, Manchester, United Kingdom

[2] Carl Zeiss X-ray Microscopy, Pleasanton, CA, USA

[3] Department of Materials Science & Metallurgy, University of Cambridge, Cambridge, UK

[4] Carl Zeiss Industrial Metrology, Brighton, MI, USA

[5] School of Chemical and Process Engineering, University of Leeds, Leeds, UK

[6] School of Life and Medical Sciences, University of Hertfordshire, Hatfield, UK

[7] Carl Zeiss Microscopy, Oberkochen, Germany

KEYWORDS: dry powder inhaler (DPI), lactose, X-ray computed tomography (XCT), X-ray microscopy (XRM), active pharmaceutical ingredient (API), Q3 structural equivalence

SUMMARY

Microstructural equivalence (Q3) for dry powder inhalers (DPIs) is complex because it involves both pre- and post-aerosolization powders and can be influenced by the DPI device and the patient's aerosolization efficiency. In this paper, we show how advanced 3D X-ray microscopy (XRM, also known as X-ray computed tomography) techniques can provide unique microstructural insights into pre-aerosolized inhalation powders. Nano-scale XRM is used to detect differences within individual lactose particles and agglomerates, including voids and intra-agglomerate size distributions. Micro-scale XRM is used to visualize and quantify lactose fines (<12 μm) within a powder bed. XRM is also used to discriminate between excipient and terbutaline sulphate particles in an inhalation blend. These advanced XRM techniques could provide valuable microstructural information to help address Q3 equivalence during bioequivalence determination in inhalation drug products.

INTRODUCTION

Demonstrating pharmaceutical equivalence and bioequivalence (BE) between a test and reference product are important requirements in the development of generic inhalation products [1]. BE is also essential to support post-approval formulation or manufacturing process changes for existing orally inhaled drug products [1]. BE is defined as the absence of a significant difference in the rate and extent to which the active ingredient reaches the site of drug action when administered at the same dose and under similar conditions [2]. For systemically acting drugs, BE is typically demonstrated using pharmacokinetic (PK) studies, comparing drug plasma concentrations between the test and reference products. However, the ability of PK studies to assess BE for locally acting inhaled drugs remains controversial because their delivery and intended action in the lung does not rely on the systemic circulation [2–6]. Instead, the US Food and Drug Administration (FDA) utilizes a weight-of-evidence approach which includes *in vitro*, PK and pharmacodynamic (PD) or clinical studies to demonstrate BE of inhalation products [2]. Alternative pathways to establish BE in these complex drug-device combination products are currently being explored.

The FDA introduced the concept of microstructural equivalence (Q3) where differences between the same components (Q1) in the same concentration (Q2) under a non-equilibrium state can be related to the arrangement of matter and/or its state of aggregation. For topical and transdermal creams, gels and suspensions, if Q1 and Q2 are identical, then the difference is considered to be due to Q3 [7]. However, inhaled therapies are more challenging because microstructural changes of the inhaled formulation are not only due to manufacturing and formulation processes, but also as a result of the aerosolization process. Thus, there is a need to investigate the microstructural relationship between both formulated and aerosolized forms of the product, in order to address Q3 equivalence in inhaled drug formulations.

ASSESSING Q3 STRUCTURAL EQUIVALENCE IN INHALED PRODUCTS

Recently Price *et al*. reported differences in the *in vitro* dissolution profiles of Advair® Diskus® and Seretide® Accuhaler® dry powder inhalers (DPIs) (GlaxoSmithKline, USA and UK) and highlighted differences in the state of aggregation of the active pharmaceutical ingredients (APIs) and excipients using morphology-direct Raman spectroscopy (MDRS) [8, 9]. Whilst this orthogonal approach using *in vitro* dissolution testing coupled with MDRS characterization can detect subtle differences in the post-aerosolized product, the role of any microstructural differences in the pre-aerosolized material that may contribute to this behavior remains unknown. Linking the microstructure of the pre-aerosolized formulation with the performance of the inhaled product is needed and some critical questions still remain unanswered: What does the microstructure of the formulation really look like? How does processing change this microstructure? And how do microstructural differences in the formulation manifest in the final aerosolization performance? With these questions in mind, the INFORM 2020 consortium was formed with funding from the United Kingdom's Engineering and Physical Sciences Research Council, bringing together academic institutions, pharmaceutical companies and technology experts to develop new techniques to characterize the Q3 microstructure.

The potential of X-ray Computed Tomography (XCT) to provide unique three-dimensional microstructural insight of pharmaceutical formulations has long been of interest [10, 11]. However, the small particle sizes associated with inhalation blends have been a major obstacle to the widespread use of the technology. Improvements in instrument technology, in particular the development of x-ray optical elements [12], over the past 10 years has allowed higher resolution

and improved contrast to be achieved on laboratory systems. Such is the level of detail provided by the x-ray optics that these XCT machines are alternatively known as x-ray microscopes, giving rise to the field of x-ray microscopy (XRM) [13, 14]. Recently, x-ray microscopes have been used as multiscale characterization tools for inhalation powders, providing information on meso-, micro- and nano-scales [15]. XRM has also been shown to quantify particle size and shape in 3D, and provide information on the number and positions of fine lactose particles in the powder bed [16]. In this paper, we show how these new XRM techniques can help unlock further microstructural features of inhalation blends.

VISUALIZING INTERNAL STRUCTURES USING PHASE-CONTRAST X-RAY MICROSCOPY (XRM)

As x-rays pass through a sample, two ways that they are affected are attenuation and diffraction [17]. First, the x-rays are attenuated, with the absorption proportional to atomic number (Z). Denser elements attenuate x-rays to a greater degree, and hence materials with different densities can be distinguished through different grayscale values within a reconstructed slice of a 3D dataset. For example, the different grayscale values within the Diskus/Accuhaler DPI shown in Figure 1 show different density materials. Second, x-rays are diffracted, i.e. the phase of the x-ray wave is shifted. The interaction between a diffraction wave and an un-diffracted wave produces characteristic white and dark fringes that are known as Fresnel fringes at the edges and boundaries in the sample where there is a change in the index of refraction [18]. Absorption scans are typically quicker than pure phase contrast scans and provide sufficient contrast in many cases. However, for low Z materials such as organic compounds including pharmaceuticals, where the differences in x-ray absorption of different phases are minimal, there is insufficient contrast to differentiate different compounds [19, 20]. The phase contrast modality is typically slower than absorption mode as the signal on the detector is weaker and additionally requires the use of dedicated Zernike phase rings [21] or a combination of highly coherent sources and large propagation distances at which the phase fringes are better resolved [18]. In the case of low Z materials, the dominant contrast mechanism is through phase shift occurring at particle boundaries or interfaces where there is a significant difference in the index of refraction, providing high contrast sensitivity to otherwise weakly absorbing features such as voids, porosity and boundaries between very similar materials [22].

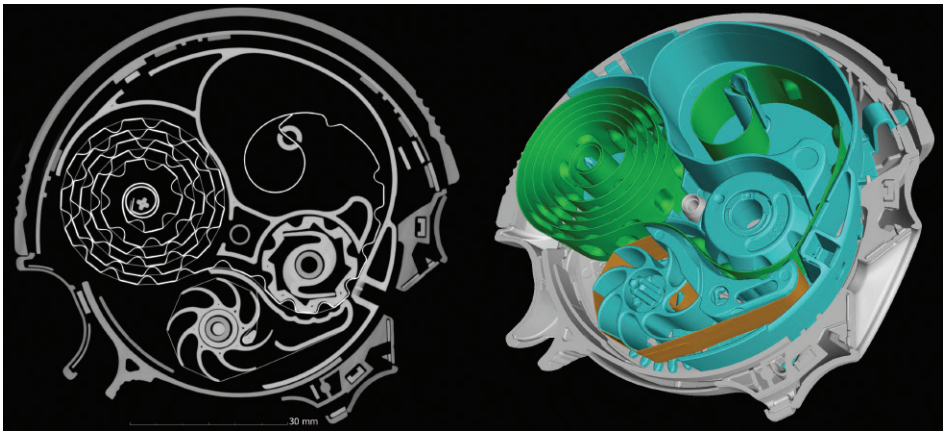

Figure 1. **An example of absorption-contrast can be seen in an XRM scan of an Accuhaler (GlaxoSmithKline, United Kingdom), with a cross-sectional virtual slice (left) and 3D rendering (right). The different grayscale values in the left panel correspond to different density materials within the inhaler.**

Figure 2 shows the same vertical cross-sectional slice from 3D reconstructions of a Lactohale 206 sample scanned using both absorption and phase-contrast modalities on a Zeiss Xradia 810 Ultra system (Carl Zeiss Microscopy, USA). The sample was prepared by mounting particles from a batch of Lactohale 206 powder (DFE Pharma, Germany) on the end of a dress-maker pin using epoxy resin. The Ultra 810 is a nano-scale XRM instrument using a monochromatic parallel x-ray beam of 5.4 keV photons, with the capability of both absorption contrast and phase-contrast modalities through a Zernike phase-ring. The Ultra system allows samples up to 64 μm to be scanned at a spatial resolution of 150 nm whilst samples smaller than 16 μm can be scanned at a 50 nm spatial resolution. The detector binning was set at 2×, with each projection image 512 × 512 pixels in size. 801 projections were collected as the sample was rotated through 360º for both scans, with Nyquist sampling theorem suggesting the number of projections should be π/2 multiplied by the projection image width [23]. The exposure time for each projection was 10 s and 30 s for the absorption-contrast and phase-contrast scans respectively. The phase-contrast modality of XRM (Figure 2B) provides greater contrast than the absorption modality (Figure 2A) allowing the identification of two separate particles separated by the epoxy. The entirety of Particle 1 is contained within the field of view, but only a part of Particle 2 can be seen. The epoxy on two sides of Particle 2 would suggest that this particle has been immersed entirely in the resin. A 3D visualization of the entire sample can be seen in Figure 2C, where two smaller particles can be seen attached to Particle 2. The phase-contrast also allows further details of the microstructure to be uncovered. Multiple line-voids were observed within the particles that appear to align in the same direction within each individual crystal. The cause of the particle voids is currently under investigation, which may be induced by sample preparation or a function of lactose manufacture. However, since the voids in Particle 1 are aligned diagonally upwards, whilst those in Particle 2 are vertical, this indicates the ability of XRM to identify intra-particulate features with their directionality based on particle orientation. Furthermore, no voids were seen within a control recrystallized lactose particle that was mounted using the same epoxy resin method (Figure 2D), indicating the potential ability of XRM to detect the impact of manufacturing process differences on particle properties. Further work is needed to test a range of different samples and lactose grades, but XRM coupled with nano-indentation could help our understanding on how these voids influence particle fracture [24].

As seen above, the Fresnel phase-contrast fringes [18] provide a sharp boundary that helps identify parts of a sample. Phase-contrast fringes were also beneficial in [16] for separating lactose particles within a bulk powder. However, in many cases phase-contrast can make segmentation (i.e. partitioning the digital image into multiple segments to identify different phases or particles) more challenging. It is worth noting that while the edges are sharply defined, the overall grayscale contrast between the air and particles is reduced in the phase contrast images (Figure 2B) compared to the absorption images (Figure 2A).

ASSESSING THE STRUCTURE OF MICRONIZED-PARTICLE AGGLOMERATES USING XRM

The structure and behavior of microparticles (both API and excipient 'fines') have been shown to play a key part in the control of aerosolization performance [25]. However, micronized particles tend to be highly cohesive and naturally form agglomerates or granular 'pseudo'-particles [26]. Knowledge of the agglomerate microstructure is important for understanding de-agglomeration, but these pseudo-particles present a major challenge for microstructural analytical techniques such as optical microscopy, scanning-electron microscopy or laser diffraction which are unable to determine the intra-agglomerate structure. The non-destructive capability of nano-scale XRM with phase-contrast modality to investigate interior particulate structures was utilized to examine a

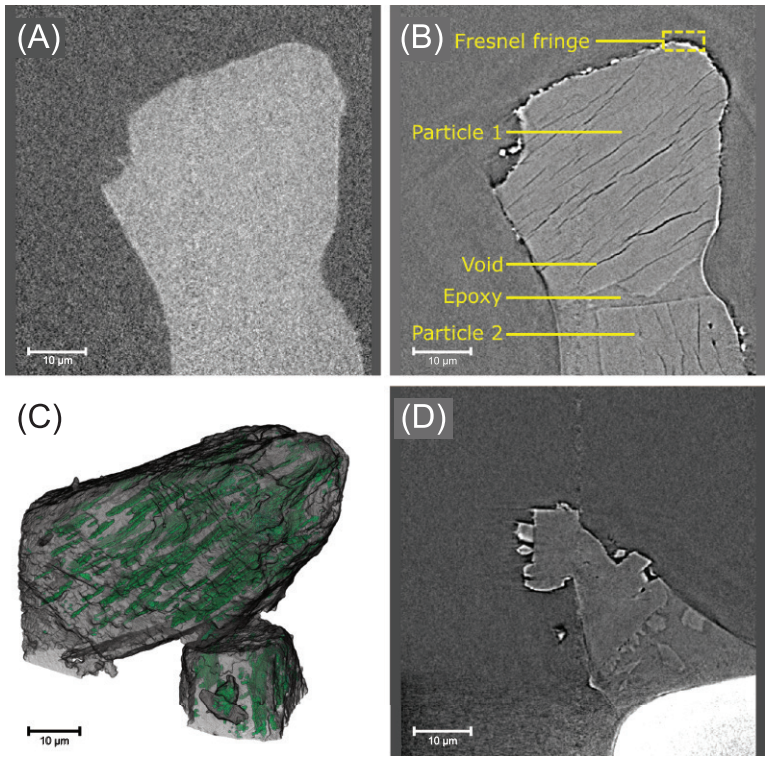

Figure 2. **Virtual vertical cross-sectional slices through reconstructions of a Lactohale 206 sample scanned with nano-XRM using (A) absorption contrast and (B) phase-contrast. (C) 3D visualization of the same Lactohale 206 sample, with the epoxy rendered transparent and the cracks shown in green. (D) Virtual vertical cross-sectional slice through a reconstruction of a control recrystallized lactose sample.**

Lactohale 300 (LH300) agglomerate. The agglomerate was mounted on the end of a dress maker pin using epoxy resin and scanned using the Zeiss Xradia Ultra 810 XRM instrument using the same phase-contrast scan settings described previously. but with an exposure time of 60 s per projection. The final 3D virtual volume was reconstructed using the proprietary Zeiss Reconstructor software.

A single cross-sectional slice through the virtual volume is shown in Figure 3A. Although the different particles within the agglomerate can be clearly seen, there is little grayscale difference between the particles and surrounding air (i.e. void space within the agglomerate) making segmentation of the lactose phase very challenging. However, post-processing the virtual volume with a proprietary phase retrieval algorithm (Carl Zeiss Microscopy, USA) minimizes the phase fringes seen along the edges and enhances the grayscale contrast as shown in Figure 3B [27]. The implementation is based on modelling the physical diffraction with an image filter model, with the phase retrieval and correction performed by de-convolving the appropriate filter function with the acquired data [28]. From the simpler dataset, the lactose phase can be easily segmented. Furthermore, individual particles within the agglomerate can be identified and thus a size-distribution of the individual, constituent micro-particles that form the agglomerate deduced as shown in Figure 3C. The distribution is bimodal, with the first mode about 0.5 µm and a second mode about 2.5 µm. The cross-sectional slice (Figure 3A) appears to show some organization between the particles, and Figure 3D shows a 3D visualization of the agglomerate with each of the particles colored by the

particle size. Further work is needed to quantify the relative spatial positions of the different sized particles within the agglomerate which could provide valuable insight into the cohesive nature of micronized powders.

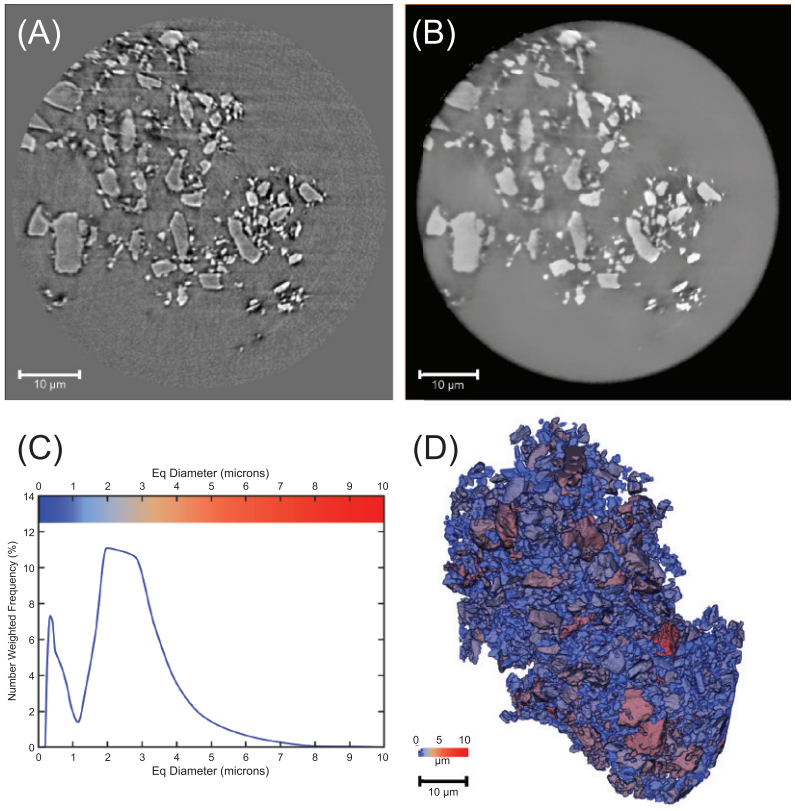

Figure 3. **(A) A single raw horizontal virtual cross-sectional slice through an LH300 agglomerate. (B) The same slice after processing using a phase-retrieval filter. Notice the distinct grayscale values between air (void space) and lactose particles. (C) Size distribution for all of the particles identified within the agglomerate. (D) 3D visualization of the LH300 agglomerate with each particle colored by its size, with the range given by the color bar in the bottom left corner of (D) and at the top of (C).**

SPATIAL DISTRIBUTION OF FINES IN INHALATION BLENDS

The addition of fine lactose particles increases the cohesiveness of a bulk lactose powder and thus reduces the powder flowability [25, 29]. Kopsch, Murnane and Symons [30] visualized the entrainment of three different lactose powders (Respitose SV003 (fine, sieved lactose), Lactohale 100 (sieved lactose) and Lactohale 200 (milled lactose); all DFE Pharma, Germany) using a high speed camera at 1000 frames per second. The entrainment behavior of Respitose SV003 and Lactohale 100 was found to be consistent, reproducible and corresponded well with CFD results. However, the fluidization behavior of Lactohale 200 was found to be chaotic, with different entrainment behavior for each run even though the experimental setup was identical. The authors acknowledged that non-reproducible entrainment behavior of Lactohale 200 could be related to the increased cohesivity of the milled lactose grade from a higher proportion of fines compared to the sieved grades Respitose SV003 and Lactohale 100 [30].

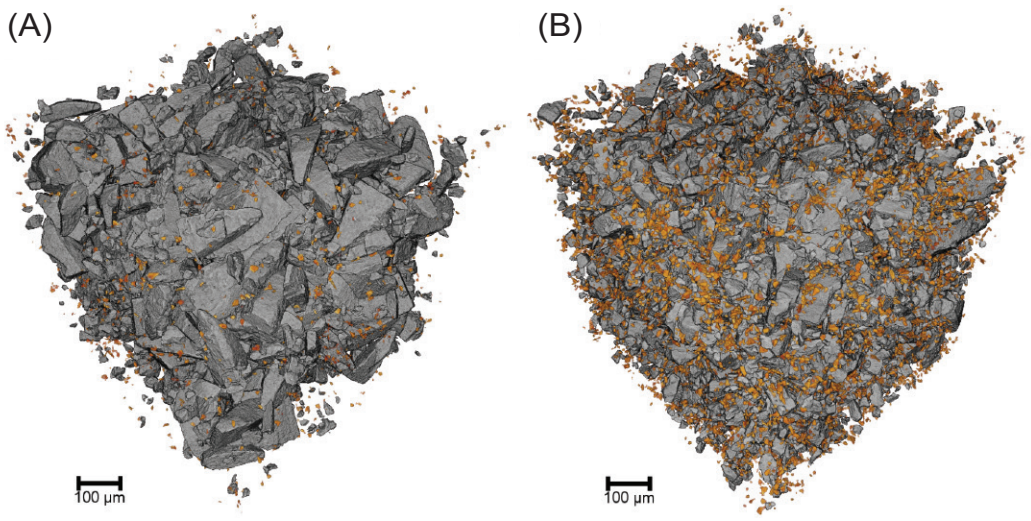

Figure 4. 3D Visualizations of (A) Lactohale 100 and (B) Lactohale 200, with particles smaller than 12 µm colored orange, and those larger than 12 µm in gray.

The spatial positions of fine particles in Lactohale 100 and Lactohale 200 for dry powder inhaler formulations have recently been reported [16]. Figure 4 shows 3D visualizations of the data from [16], with particles less than 12 µm in size colored orange and those larger than 12 µm in gray. Furthermore, it was possible to quantify the number of sub-12 µm fines by identifying eight non-overlapping regions of interest (ROI) within the full analysis volume and counting the number of fines in ROI. Dividing by the volume of the ROI gave the number density, with Lactohale 100 containing 9426 ± 559 particles per mm^3 and Lactohale 200 containing 66458 ± 6033 particles per mm^3. Whilst Lactohale 200 has more than seven times as many fines compared to Lactohale 100, the high spatial variation in the number of fines could offer an explanation for the inconsistent entrainment behavior. Further work is underway to quantify the number of fines across a range of powders and link this to other physical properties.

REVEALING MULTIPLE SPECIES IN INHALATION BLENDS

The key component of an inhalation blend is the API, and effective de-agglomeration of the drug from the carrier particles is critical to the performance. De-agglomeration is linked to the spatial interactions of drug and excipient and XRM could be a useful exploratory tool due its intrinsic three-dimensional nature. A blend of Capsulac 60 (Meggle, Germany) and terbutaline sulphate (TBS) in a 9:1 mass ratio was mixed using a Turbula mixer (Willy A Bachofen, Basel, Switzerland) at a frequency of 30 Hz for 1 h. Capsulac 60, a tableting grade lactose, was chosen as a model carrier in the blend due to its larger size. The TBS-Capsulac 60 blend was loaded by hand into a Kapton tube sample holder [15] and scanned using a Zeiss Xradia Versa 520 micro-XRM instrument (Carl Zeiss Microscopy, USA). A 10× objective lens was used, with 2× detector binning and source-to-sample and sample-to-detector distances of 12 mm and 14 mm respectively, giving a reconstructed voxel size of 1.27 μm^3. As the size of each projection was 1005 × 1005 pixels, 1601 projections were collected as suggested by the Nyquist sampling theorem. Each projection had a 12.5 s exposure time. A voltage of 40 kV and current of 75 µA was used to maximize any absorption contrast between

the different density Capsulac 60 and TBS. The Versa system produces in-line phase contrast due to the highly coherent source, and thus the final volume contains some absorption contrast along with Fresnel fringes.

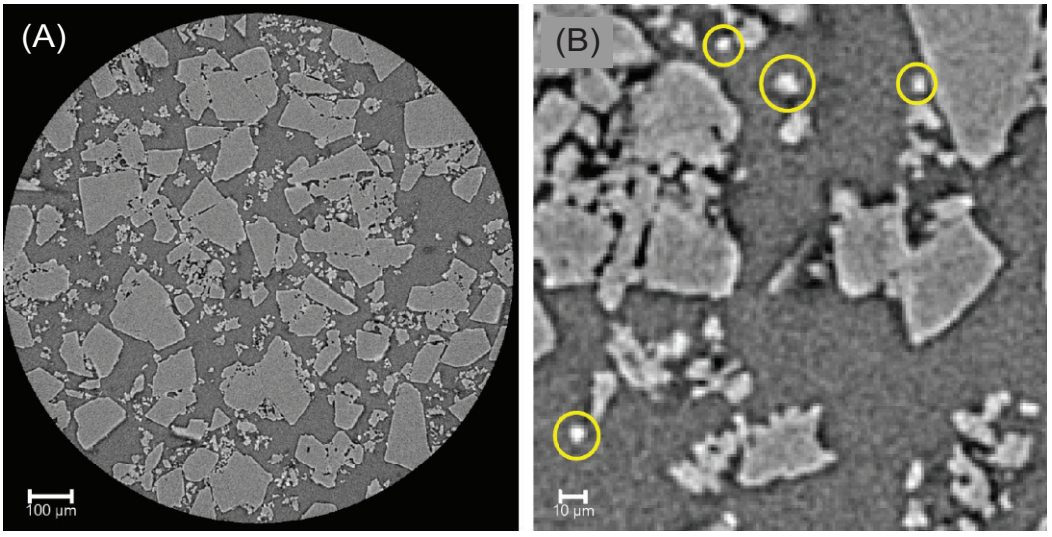

Figure 5. **(A) Virtual horizontal cross-sectional slice through the blend of terbutaline sulphate and Capsulac 60. (B) A zoomed section of the same slice with several particles highlighted that have uncharacteristically bright grayscale color.**

Figure 5A shows a single cross-sectional slice through the virtual volume. Although the Fresnel fringes can be seen at the edges of particles that reveal the particle boundaries in detail, they alone are not sufficient in the identification of the two species. In fact, in some cases they may pose additional difficulties in the phase identification. X-ray absorption is proportional to material density and since the densities follow air (0.001 kg/L) < TBS (1.18 kg/L) < lactose (1.54 kg/L), the grayscale values should also follow with air being the darkest and lactose the lightest. However, Figure 5B shows a zoomed section of the cross-sectional slice with several example small particles circled, where the grayscale value is brighter than the surrounding lactose. This is due to the bright ring from the Fresnel fringe making the grayscale value across the entire small particle very bright. Thus, from the raw reconstructed volume alone, it is extremely challenging to distinguish between the lactose and TBS that are both low Z materials with only small density differences.

After post-processing the raw reconstructed data with the phase-retrieval algorithm (to minimize phase fringes seen at particle boundaries and enhance grayscale contrast), there are distinct grayscale values for the two species allowing particles of each to be identified. Figure 6A shows a 3D visualization with Capsulac 60 colored gray and TBS colored green, with the proportion of TBS calculated to be 8.1%. Although this is lower than the expected proportion of 10% TBS in the blend, this may be due to segregation and/or errors in identifying the two species. It is possible to verify the segmentation by obtaining size-distributions of the two phases, as shown in Figure 6B. The size distribution of the TBS phase is less than 75 µm, whilst that of Capsulac 60 is between 100 and 400 µm. The size distribution of Capsulac 60 identified in the blend is slightly different from that of pure Capsulac 60 analyzed in [16] and plotted here for comparison. Although the size range is broadly similar, the distribution determined from the

blend has a bimodal distribution. This could be due to powder aggregates breaking up during the blending process. Examining the morphology of the two phases, the Capsulac 60 particles have the characteristic lactose tomahawk shape [31], sometimes with particles aggregated together as shown in Figure 6C. By contrast, the identified TBS particles have a plate-like morphology [32] as shown in Figure 6D. Further work is currently underway to improve the particle separation and extend the technique to blends containing inhalation grade lactose. Although the results are promising, it will be necessary to validate the identification of different chemical species using the phase retrieval algorithm by comparison to existing techniques such as Energy-dispersive X-ray spectroscopy (EDX). Note that EDX requires dispersion of the powder sample whilst XRM is the only technique able to look inside a bulk powder.

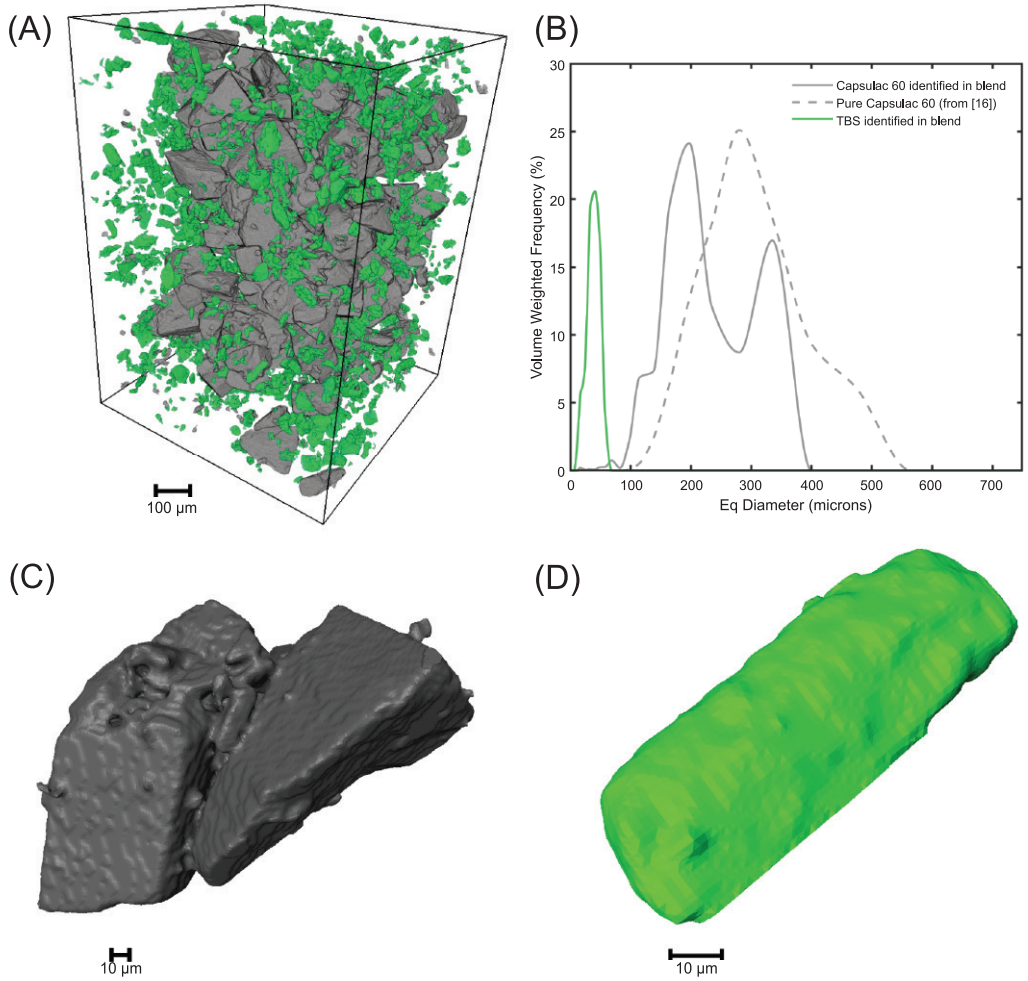

Figure 6. **(A) 3D visualization of Capsulac 60 – TBS blend, with Capsulac 60 colored gray and TBS colored green. (B) Size distribution of the two identified phases, with pure Capsulac 60 plotted alongside for comparison. Pure Capsulac 60 data reproduced from Gajjar *et al.* [16] under a Creative Commons Attribution 4.0 International License (http://creativecommons.org/licenses/by/4.0/). (C) Typical Capsulac 60 morphology, showing the characteristic tomahawk shape arranged in an aggregate. (D) Typical plate-like TBS morphology.**

CONCLUSIONS

X-ray microscopy with phase-contrast modality has the potential to provide unique insight into the microstructure of pre-aerosolized DPI formulations. Nano-scale XRM allows internal features, e.g. voids, of individual particles to be revealed. This level of detail is unrivalled and could allow direct comparisons between batch-to-batch and site-to-site manufacturing variability. Furthermore, nano-scale XRM allows quantification of microstructural features within agglomerates such as the internal particle size distribution. If other information such as porosity and contact areas can also be extracted, then nano-scale XRM could provide a valuable link between the pre- and post-aerosolized product. Micro-scale XRM allows individual drug and excipient particles to be identified within a powder sample. Unique to XRM is that it is non-destructive, potentially opening doors as a process analytical technology (PAT) [33] for production line assessment of formulations within capsules and blisters. Further work is certainly needed, but promising early signs are that XRM could potentially unlock the assessment of microstructure of inhaled formulations and provide a bridge between Q3 and BE studies.

ACKNOWLEDGEMENTS

The authors of this paper are members of the INFORM 2020 Consortium, which is funded through EPSRC grant EP/N025075/1. We are grateful to consortium partners DFE Pharma and Meggle for the supply of the raw materials, and further acknowledge 3M, AstraZeneca, GlaxoSmithKline, Carl Zeiss Microscopy and Malvern Panalytical for their membership and support of the INFORM 2020 Consortium. Beam-time was kindly provided by the Henry Moseley X-ray Imaging Facility (HMXIF), which was established through EPSRC Grant Nos. EP/F007906/1, EP/I02249X/1, and EP/F028431/1. HMXIF is a part of the Henry Royce Institute for Advanced Materials, established through EPSRC Grant Nos. EP/R00661X/1, EP/P025498/1, and EP/P025021/1.

REFERENCES

1. Lu D, Lee SL, Lionberger RA, Choi S, Adams W, Caramenico HN *et al.*: International guidelines for bioequivalence of locally acting orally inhaled drug products: Similarities and differences. *AAPS J* 2015, 17: 546–57.

2. Saluja B, Li BV, Lee SL: Bioequivalence for orally inhaled and nasal drug products. In *FDA Bioequivalence Stand.* Edited by Yu LX, Li BV. Springer; New York, NY: 2014: 369–94.

3. Usmani OS, Molimard M, Gaur V, Gogtay J, Singh GJP, Malhotra G *et al.*: Scientific rationale for determining the bioequivalence of inhaled drugs. *Clin Pharmacokinet* 2017, 56: 1139–54.

4. Hochhaus G, Horhota S, Hendeles L, Suarez S, Rebello J: Pharmacokinetics of orally inhaled drug products. *AAPS J* 2015, 17: 769–75.

5. Evans C, Cipolla D, Chesworth T, Agurell E, Ahrens R, Conner D *et al.*: Equivalence considerations for orally inhaled products for local action – ISAM/IPAC-RS European Workshop Report. *J Aerosol Med Pulm Drug Deliv* 2012, 25: 117–39.

6. O'Connor D, Adams WP, Chen M-L, Daley-Yates P, Davis J, Derendorf H *et al.*: Role of pharmacokinetics in establishing bioequivalence for orally inhaled drug products: Workshop Summary Report. *J Aerosol Med Pulm Drug Deliv* 2011, 24: 119–35.

7. Kryscio DR, Sathe PM, Lionberger R, Yu L, Bell MA, Jay M *et al.*: Spreadability measurements to assess structural equivalence (Q3) of topical formulations – a technical note. *AAPS PharmSciTech* 2008, 9: 84–6.

8. Price R, Farias G, Ganley W, Shur J: Demonstrating Q3 structural equivalence of dry powder inhaler blends: New analytical concepts and techniques. In *Respiratory Drug Delivery 2018*. Volume 1. Edited by Dalby RN, Byron PR, Hindle M, Peart J, Traini D, Young PM, Farr SJ, Suman JD, Watts A. DHI Publishing; River Grove, IL: 2018; 265–276.

9. Price R, Farias G, Ganley W, Shur J: Challenging the bioequivalence hurdles for OINDPs: Achieving Q3 structural equivalence. In *Respiratory Drug Delivery Asia 2018*. Edited by Dalby RN, Peart J, Traini D, Young PM. DHI Publishing; River Grove, IL: 2018: 1–14.

10. Fu X, Elliott JA, Bentham AC, Hancock BC, Cameron RE: Application of X-ray micro-tomography and image processing to the investigation of a compacted granular system. *Part Part Syst Charact* 2006, 23: 229–36.

11. Shur J, Price R: Advanced microscopy techniques to assess solid-state properties of inhalation medicines. *Adv Drug Deliv Rev* 2012, 64: 369–82.

12. Gelb J: Functionality to failure: Materials engineering in the 4th dimension. *Adv Mater Process* 2012, 170: 14–8.

13. Merkle AP, Gelb J: The ascent of 3D X-ray microscopy in the laboratory. *Micros Today* 2013, 21: 10–15.

14. Lavery LL, Gelb J, Merkle AP, Steinbach A: X-ray microscopy for hierarchical multi-scale materials. *Micros Today* 2014, 22: 16–21.

15. Gajjar P, Styliari ID, Burnett TL, Chen X, Elliott JA, Ganley WJ *et al.*: Multiscale tomography: Probing the nano-, micro-, and meso-scale resolution of inhalation powder structure. In: *Respiratory Drug Delivery Europe 2019*. Edited by Dalby RN, Peart J, Suman D, Traini D, Young PM. DHI Publishing; River Grove, IL: 2019: 155–68.

16. Gajjar P, Styliari ID, Nguyen TTH, Carr J, Chen X, Elliott JA *et al.*: 3D characterisation of dry powder inhaler formulations: Developing X-ray micro computed tomography approaches. *International Journal of Pharmaceutics* 2020, Jan 11:118988. doi: 10:1016/j.ijpharm.2019.118988. [Epub ahead of print].

17. Chen G-H, Zambelli J, Bevins N, Qi Z, Li K: X-ray phase sensitive imaging methods: Basic physical principles and potential medical applications. *Curr Med Imaging Rev* 2010, 6: 90–9.

18. Wilkins SW, Gureyev TE, Gao D, Pogany A, Stevenson AW: Phase-contrast imaging using polychromatic hard X-rays. *Nature* 1996, 384: 335–8.

19. Momose A, Takeda T, Itai Y: Phase-contrast X-ray computed tomography for observing biological specimens and organic materials. *Rev Sci Instrum* 1995, 66: 1434–6.

20. Momose A, Takeda T, Itai Y, Hirano K: Phase-contrast X-ray computed tomography for observing biological soft tissues. *Nat Med* 1996, 2: 473–5.

21. Holzner C, Feser M, Vogt S, Hornberger B, Baines SB, Jacobsen C: Zernike phase contrast in scanning microscopy with X-rays. *Nat Phys* 2010, 6: 883–7.

22. Mayo SC, Stevenson AW, Wilkins SW: In-line phase-contrast X-ray imaging and tomography for materials science. *Materials* 2012, 5: 937–65.

23. Buzug T: *Technical implementation. Computed Tomography – From Phot Stat to Mod Cone-Beam CT*. Springer. Berlin Heidelberg: 2008, 241–301.

24. Patterson BM, Cordes NL, Henderson K, Mertens JCE, Clarke AJ, Hornberger B *et al.*: In situ laboratory-based transmission X-ray microscopy and tomography of material deformation at the nanoscale. *Exp Mech* 2016, 56: 1585–97.

25. Kinnunen H, Hebbink G, Peters H, Shur J, Price R: An investigation into the effect of fine lactose particles on the fluidization behaviour and aerosolization performance of carrier-based dry powder inhaler formulations. *AAPS PharmSciTech* 2014, 15(4): 898–909.

26. Le VNP, Robins E, Flament MP: Agglomerate behaviour of fluticasone propionate within dry powder inhaler formulations. *Eur J Pharm Biopharm* 2012, 80: 596–603.

27. Thompson DA, Nesterets YI, Pavlov KM, Gureyev TE: Fast three-dimensional phase retrieval in propagation-based X-ray tomography. *J Synchrotron Radiat* 2019, 26: 825–38.

28. Wernersson ELG, Boone M, Van den Bulcke J, Van Hoorebeke L, Luengo Hendriks CL: Understanding phase contrast artefacts in micro computed absorption tomography. In SSBA Symposium Proceedings. *Swedish Society for Automated Image Analysis (SSBA)*. Luleå, Sweden: 2014, 6.

29. Finlay WH: *The mechanics of inhaled pharmaceutical aerosols: An introduction*. Elsevier Science. Amsterdam: 2001.

30. Kopsch T, Murnane D, Symons D: Computational modelling and experimental validation of drug entrainment in a dry powder inhaler. *Int J Pharm* 2018, 553: 37–46.

31. Zeng XM, Martin GP, Marriott C, Pritchard J: The influence of crystallization conditions on the morphology of lactose intended for use as a carrier for dry powder aerosols. *J Pharm Pharmacol* 2000, 52: 633–43.

32. Nguyen TTH, Hammond RB, Styliari ID, Murnane D, Roberts KJ: A digital workflow from crystallographic structure to single particle attributes for predicting the formulation properties of terbutaline sulphate. *Int J Pharm* 2020. Submitted.

33. Miller JD, Lin CL: Opportunities for plant-site 3D coarse particle characterization with automated high-speed X-ray tomography. *Miner Metall Process* 2016, 33: 53–7.